Theoretical Study of the Small Slope Approximation for Ocean Polarimetric Thermal Emission

Joel T. Johnson, *Member, IEEE,* and Min Zhang

***Abstract*— Analytical models for ocean surface polarimetric thermal emission based on the small perturbation method (SPM) have shown success in matching brightness temperature azimuthal variations from aircraft based measurements. It has also been shown that use of the small perturbation method for calculation of surface emissivity results in a series in surface slope, not surface height, so that the method remains accurate for large height surface emission even when it fails for the corresponding scattering calculations. This paper presents a detailed analysis of the SPM/small slope approximation (SPM/SSA) for ocean surface polarimetric thermal emission, and investigates the extent to which varying ocean surface length scales contribute to brightness temperature zeroth and second azimuthal harmonics. It is found that ocean waves of lengths both comparable to and much greater than the electromagnetic wavelength can contribute to these harmonics, depending on the extent to which the ocean surface spectral model places asymmetry in these length scales. In addition, the SPM/SSA is approximated for the contributions of both very long and very short ocean length scales compared to the electromagnetic wavelength, and it is found that both long and short wave contributions can be expressed in simple equations involving either standard or modified ocean surface slope variances.**

***Index Terms*—Microwave readiometry, passive remote sensing.**

I. Introduction

RECENT experimental and theoretical studies have demonstrated the utility of polarimetric techniques in microwave passive remote sensing of ocean wind speed and direction [1]–[7]. The success of these studies has resulted in plans for a polarimetric radiometer to be included in the NPOESS series of satellites [8]. Analytical and numerical models for the calculation of ocean surface polarimetric thermal emission have also been developed [9]–[13], primarily through application of standard surface scattering approximate methods to calculate surface emissivity using Kirchhoff's law. Models based on both the small perturbation method (SPM) and the physical optics (PO) approximation have been presented, as well as some limited numerical studies of short gravity/capillary wave emission with the method of moments [14]. A recent work [12] has further revealed that use of the SPM for emission calculations results in a small slope, rather than small height, emission approximation identical to that which would be obtained from the small slope approximation of [15], so that the SPM can provide accurate emission predictions even for surfaces with large heights in terms of the electromagnetic wavelength. Numerical tests of the SPM for a set of canonical periodic surfaces have confirmed this statement [16]. These results motivate use of the SPM/small slope approximation (SPM/SSA) for the study of ocean polarimetric thermal emission since ocean surface slopes are often relatively small on average.

Although the SPM/SSA has been applied in several previous studies of ocean emission [5], [9]–[10], obtaining insight into the emission process through this technique remains difficult due to the integration of bistatic scattering coefficients required in Kirchhoff's law. Furthermore, calculation of brightness temperatures requires that a model for the ocean surface directional spectrum be included, and the particular spectral model chosen can strongly influence the results obtained. For these reasons, several questions remain [17] regarding the underlying sources of observed ocean emission azimuthal harmonics, and in particular the influence of ocean surface features of length scales much larger than or comparable to the electromagnetic wavelength.

In this paper, an attempt to resolve some of these questions is made through a detailed study of the SPM/SSA. The SPM/SSA formulation of [9] is followed, but the resulting equations are simplified and re-written in a form which is more amenable to interpretation. It is found that brightness temperature azimuthal harmonics for each polarimetric quantity can be written as an integral of a weighting function over the corresponding surface curvature spectrum azimuthal harmonic. Studies of the harmonic weighting functions reveal them to have a simple behavior for ocean length scales much larger than or much shorter than the electromagnetic wavelength, and approximations for these limits are derived and presented. Overall results again confirm the small slope series of the method, and show that ocean surface length scales both comparable to or much larger than the electromagnetic wavelength can contribute to brightness temperature azimuthal harmonics. Studies of the weighting functions allow the influence of a particular ocean surface spectral model to be removed, so that clearer insight into the emission physics of the SPM/SSA can be obtained. In addition to providing insight, the techniques presented offer a means for more rapid and direct calculation of emission harmonics than previous integration techniques.

It is noted that the SPM/SSA studied in this paper involves only second order terms in surface slope, so that no first azimuthal harmonics of the emission are obtained. As shown in reference [13], a consistent analysis of the first harmonic requires that third order terms in surface slope be retained, but the complexity of these terms has limited previous analyses to approximate studies only. A heuristic prediction of first

Manuscript received September 16, 1998; revised May 1, 1999. This work was supported by the Office of Naval Research under Contract N00014-97-1-0541.

The authors are with the Department of Electrical Engineering and Electro-Science Laboratory, The Ohio State University, Columbus, OH 43210 USA (e-mail: johnson@ee.eng.ohio-state.edu).

Publisher Item Identifier S 0196-2892(99)06968-5.

harmonics with the SPM/SSA can be obtained through a "tilting" procedure [10], but such an approach is not followed in this paper due to the ambiguity in choice of the "cutoff" wavenumber for a small slope theory. Furthermore, the influence of surface foam and atmospheric emission are not considered, although both can potentially contribute to azimuthal variations of measured brightness temperatures [11].

The next section briefly reviews the SPM/SSA for ocean surface emission, and a simplified expression for the theory is derived in Section III. The "weighting" functions in this expression are then studied in more detail in the Section IV, and analytical expressions for long and short wave contributions are then presented in the following sections. A final discussion of the results presented concludes the paper.

II. SPM/SSA for Ocean Emission Calculations

Polarimetric passive remote sensing involves measurement of all four modified Stokes parameters of the microwave thermal emission

$$\overline{T}_B = \begin{bmatrix} T_{Bh} \\ T_{Bv} \\ T_U \\ T_V \end{bmatrix} = T_s \left(\begin{bmatrix} 1 - r_h \\ 1 - r_v \\ -r_U \\ -r_V \end{bmatrix} \right) \tag{1}$$

where T_{Bh} and T_{Bv} are the brightness temperatures measured by horizontally and vertically polarized antennas respectively, and T_U and T_V are proportional to the real and imaginary parts of the correlation between fields in horizontal and vertical polarizations respectively [9]. The second equality follows from Kirchhoff's Law, which relates the emissivity of a medium at constant temperature to the corresponding reflectivity (r_h, r_v, r_U, and r_V) multiplied with the surface physical temperature T_s. Reflectivities are calculated as an integral of bistatic scattering coefficients over the upper hemisphere in the reciprocal active scattering problem [18].

Particular interest in ocean wind remote sensing is given to brightness temperature variations in azimuth, and it is convenient to represent these variations in terms of a set of azimuthal harmonics. Due to the statistical reflection symmetry of an ocean surface about the wind direction, it can be shown [19] that an appropriate expansion is

$$\begin{bmatrix} T_{Bh} \\ T_{Bv} \\ T_U \\ T_V \end{bmatrix} \approx \begin{bmatrix} T_{Bh}^{(0)} + T_{Bh}^{(1)} \cos\phi_i + T_{Bh}^{(2)} \cos 2\phi_i \\ T_{Bv}^{(0)} + T_{Bv}^{(1)} \cos\phi_i + T_{Bv}^{(2)} \cos 2\phi_i \\ T_U^{(1)} \sin\phi_i + T_U^{(2)} \sin 2\phi_i \\ T_V^{(1)} \sin\phi_i + T_V^{(2)} \sin 2\phi_i \end{bmatrix} \tag{2}$$

where ϕ_i denotes the azimuth angle between the radiometer look direction and wind direction. The azimuthal harmonic coefficients, $T_\gamma^{(i)}$, remain functions of the radiometer polar observation angle θ_i, the frequency of observation f, the relative permittivity of sea water ϵ, and the statistical properties of the surface.

The SPM/SSA applies standard small perturbation theory to predict the bistatic scattering coefficients of a rough surface, and integrates these scattering coefficients over the upper hemisphere to obtain the reflectivities and hence brightness temperatures. It is well known that the SPM for scattering predictions produces a series in surface height relative to the electromagnetic wavelength, so that the approach converges well only for surfaces with small rms heights in terms of the electromagnetic wavelength (an accepted definition for first order SPM is that the height should be less than approximately $\lambda/20$, where λ is the electromagnetic wavelength [20]). However, the rms height of an ocean surface at microwave frequencies can be much larger than $\lambda/20$, so use of the SPM for scattering predictions becomes invalid, particularly in the near specular region where the largest scattering cross sections are obtained. Since calculation of emissivity requires that all bistatic scattering cross sections be integrated, inaccuracies in the largest scattering cross sections make the accuracy of the SPM for emission calculations seem questionable. These considerations resulted in only short gravity and capillary wave contributions (ocean length scales within an order of magnitude of the 2.14-cm electromagnetic wavelength studied) being considered in [9], since a spectral "cutoff" wavenumber was chosen below which long wave contributions were neglected. Later works [10] modeled long wave effects through a composite surface type approach, but again, choice of a spectral "cutoff" to separate the long and short scale contributions was required. However, predictions of the short gravity/capillary wave model alone were found to be in good agreement with measured brightness temperature azimuthal harmonics, and long wave contributions were found to have little influence on these results, seemingly demonstrating that only ocean length scales comparable to the electromagnetic wavelength are significant in generating brightness harmonics. It should also be noted that these predictions were obtained with the Durden–Vesecky ocean directional spectrum model [21], derived to match measured ocean scattering cross sections through the composite surface scattering model.

Questions involving use of the SPM for ocean surface emission calculations were resolved in [12], in which expressions obtained from the SPM for surface emissivity were shown to have the form of a small-slope, and not small height, approximation. Therefore, the SPM/SSA can be used for emission studies even when it fails for scattering calculations due to the small height limitation. Numerical tests with canonical periodic surfaces have confirmed this statement [16]; it is found that errors in scattering cross sections in the near specular region are compensated by errors outside of the specular region, so that the integration still produces an accurate emission prediction. Choice of a "cutoff" wavenumber based on the SPM small height limitation is therefore not required in emission studies, and the SPM/SSA can be applied to the entire ocean spectrum. A "tilting" procedure to model long wave effects is also not required since the theory should be applicable to all ocean length scales so long as they have small slopes.

Use of the SPM/SSA produces an expansion in surface slope, with zeroth order terms reproducing flat surface emission results, first order terms identically zero, and second order terms providing the first prediction of changes from flat surface brightnesses. Second order terms take the form of an integral of a set of weighting functions over the surface directional spectrum. Properties of the directional spectrum result in no first harmonic variations being obtained; a third order SPM/SSA expansion is required to obtain first harmonics. Only the second order expansion is considered.

Second order scattering cross sections in the SPM result from the standard incoherent Bragg scatter terms, plus a contribution from the second order correction to the flat surface coherent reflection coefficient. Emission contributions for both of these terms are expressed as an integral over the surface directional spectrum, and were discussed separately in [9]. Following [9], but combining these two terms into one expression results in the following form for surface brightness temperatures:

$$\begin{bmatrix} T_{Bh} \\ T_{Bv} \\ T_U \\ T_V \end{bmatrix} = T_s \left(\begin{bmatrix} 1-|R_{hh}^{(0)}|^2 \\ 1-|R_{vv}^{(0)}|^2 \\ 0 \\ 0 \end{bmatrix} - \int_0^\infty dk_\rho' \, k_\rho' \cdot \int_0^{2\pi} d\phi' W(k_\rho', \phi') \begin{bmatrix} g_h(f,\theta_i,\phi_i,\epsilon,k_\rho',\phi') \\ g_v(f,\theta_i,\phi_i,\epsilon,k_\rho',\phi') \\ g_U(f,\theta_i,\phi_i,\epsilon,k_\rho',\phi') \\ g_V(f,\theta_i,\phi_i,\epsilon,k_\rho',\phi') \end{bmatrix} \right) \tag{3}$$

where $R_{hh}^{(0)}$ and $R_{vv}^{(0)}$ are the horizontally and vertically polarized flat surface Fresnel reflection coefficients respectively, $W(k_\rho', \phi')$ is the surface directional spectrum (defined so that an integral over the k_ρ', ϕ' plane yields the surface height variance σ^2), and the g_γ "weighting" functions are given by

$$g_h(f,\theta_i,\phi_i,\epsilon,k_\rho',\phi') = 2\,\mathrm{Re}\{R_{hh}^{(0)*} f_{hh}^{(2)}\} + \frac{k_{zi}}{k_z}\,[|f_{hh}^{(1)}|^2 + |f_{hv}^{(1)}|^2]F \tag{4}$$

$$g_v(f,\theta_i,\phi_i,\epsilon,k_\rho',\phi') = 2\,\mathrm{Re}\{R_{vv}^{(0)*} f_{vv}^{(2)}\} + \frac{k_{zi}}{k_z}\,[|f_{vv}^{(1)}|^2 + |f_{vh}^{(1)}|^2]F \tag{5}$$

$$g_U(f,\theta_i,\phi_i,\epsilon,k_\rho',\phi') = 2\,\mathrm{Re}\{(R_{hh}^{(0)*} - R_{vv}^{(0)*}) f_{hv}^{(2)}\} + \frac{2k_{zi}}{k_z}\,\mathrm{Re}\{f_{vh}^{(1)} f_{hh}^{(1)*} + f_{vv}^{(1)} f_{hv}^{(1)*}\}F \tag{6}$$

$$g_V(f,\theta_i,\phi_i,\epsilon,k_\rho',\phi') = 2\,\mathrm{Im}\{(R_{hh}^{(0)*} + R_{vv}^{(0)*}) f_{hv}^{(2)}\} + \frac{2k_{zi}}{k_z}\,\mathrm{Im}\{f_{vh}^{(1)} f_{hh}^{(1)*} + f_{vv}^{(1)} f_{hv}^{(1)*}\}F. \tag{7}$$

In the above equations, Re and Im represent the real and imaginary part operators respectively, $k = 2\pi/\lambda$, $k_{zi} = k\cos\theta_i$, and $f_{\alpha\beta}^{(1)}$ and $f_{\alpha\beta}^{(2)}$ are the first and second order SPM scattering coefficients, respectively, as given in [9] with some modifications described below. The first terms in the above g_γ expressions represent the second order coherent reflection coefficient contributions, while the second terms represent the incoherent Bragg scatter contributions. Second order scattering coefficients are exactly those taken from [9], with the variables k_x, k_y, and k_z in [9, App. 3] given by $k_x = k_{xi} + k_\rho' \cos\phi'$, $k_y = k_{yi} + k_\rho' \sin\phi'$, and $k_z = \sqrt{k^2 - k_x^2 - k_y^2}$, where $k_{xi} = k\sin\theta_i\cos\phi_i$ and $k_{yi} = k\sin\theta_i\sin\phi_i$. Note that $f_{hv}^{(2)}$ is used with g_U and g_V as opposed to $f_{vh}^{(2)}$ in [9] due to an evaluation of the second order reflection coefficient in scattered field coordinates. First order coefficients are as given in [9, App. 2], except that the incident (k_{xi}, k_{yi}, k_{zi}) and scattered (k_x, k_y, k_z) variables are first interchanged and then the above equations used to represent k_x, etc. in terms of k_{xi}, k_ρ' and ϕ'.

The integral in (3) for brightness temperatures is over all length scales of the ocean spectrum (k_ρ' from 0 to ∞); however, the integration of incoherent scattering coefficients should be limited to only those length scales which produce a propagating Bragg scattered wave. The function F in the second terms of (4)–(7) indicates this fact: F is defined to be 1 for k_z real, 0 for k_z complex, and limits the incoherent contributions to waves propagating in the upper hemisphere.

Evaluation of (3) is performed through numerical integration of the double integral for fixed values of all the radiometer and surface parameters [f, θ_i, ϕ_i, ϵ, and $W(k_\rho', \phi')$]. Typical formulations based on [9] would numerically calculate double integrals for the coherent and incoherent contributions separately; the above expression combines both into one integration. This is important because the coherent and incoherent terms when calculated separately for large height surfaces can both obtain very large values which cancel when combined to yield the total emission prediction. This cancellation effect results in extremely high accuracy required in the separate numerical integrations. Combining the two into one double integral eliminates this problem.

Since evaluation of (3) results in a brightness vector for one value of ϕ_i only, studies of brightness temperature azimuthal harmonics require repeated evaluation of the double integral for varying values of ϕ_i to produce functions of azimuth. Harmonic coefficients can then be extracted from these functions through a Fourier transform. Calculation of brightness temperature azimuthal harmonic coefficients and their variations with other surface and radiometer parameters can therefore be quite time consuming.

III. Simplification of SPM/SSA

To address these issues, several properties of the original g_γ functions and the surface directional spectrum can be used. First, it is widely accepted that the ocean surface spectrum should vary as $1/k_\rho'^4$ for large values of k_ρ'; it is advantageous to remove this dependency through use of the ocean curvature spectrum, $C(k_\rho', \phi')$, defined as $k_\rho'^4 W(k_\rho', \phi')$. Next it is noted that the g_γ functions have a k^2 dependence on frequency which can be factored out by defining

$$\tilde{g}_\gamma\left(\theta_i,\phi_i,\epsilon,\frac{k_\rho'}{k},\phi'\right) = \frac{1}{k^2} g_\gamma(f,\theta_i,\phi_i,\epsilon,k_\rho',\phi') \tag{8}$$

with the resulting $\tilde{g}_\gamma$ functions depending on frequency only through k_ρ'/k. Using these ideas and re-writing the second order change in brightnesses from a flat surface (ΔT_γ) in terms of $\beta = k_\rho'/k$ yields

$$\begin{bmatrix} \Delta T_{Bh} \\ \Delta T_{Bv} \\ \Delta T_U \\ \Delta T_V \end{bmatrix} = -T_s \left(\int_0^\infty d\beta \int_0^{2\pi} d\phi' \; C(k\beta,\phi') \cdot \begin{bmatrix} g_h'(\theta_i,\phi_i,\epsilon,\beta,\phi') \\ g_v'(\theta_i,\phi_i,\epsilon,\beta,\phi') \\ g_U'(\theta_i,\phi_i,\epsilon,\beta,\phi') \\ g_V'(\theta_i,\phi_i,\epsilon,\beta,\phi') \end{bmatrix} \right) \tag{9}$$

where

$$g'_\gamma(\theta_i,\phi_i,\epsilon,\beta,\phi')\,d\beta = \frac{1}{\beta^3}\,\tilde{g}_\gamma\left(\theta_i,\phi_i,\epsilon,\frac{k'_\rho}{k}=\beta,\phi'\right)d\beta \quad (10)$$

$$= \frac{k^2}{k'^3_\rho}\left[\frac{1}{k^2}g_\gamma(f,\theta_i,\phi_i,\epsilon,k'_\rho=k\beta,\phi')\right]dk'_\rho \quad (11)$$

and the new g'_γ functions have no explicit dependence on frequency. Note that the above equation shows that the effect of changes in frequency is simply to modify $C(k\beta,\phi')$, i.e., to modify the ocean length scale which is weighted by a particular value of $g'_\gamma(\beta)$, assuming that ϵ remains constant with changes in frequency.

A second simplification is used to separate individual azimuth harmonics of the emission vector. First a study of the g'_γ functions reveals them to be functions of $\phi_i-\phi'$ alone, and not ϕ_i and ϕ' separately. This motivates expansion of the g' functions in a Fourier series as

$$g'_\gamma(\theta_i,\phi_i,\epsilon,\beta,\phi') = \sum_{n=-\infty}^{\infty} e^{in(\phi_i-\phi')}g'_{\gamma,n}(\theta_i,\epsilon,\beta). \quad (12)$$

Consideration of the fact that the g'_γ functions are real functions and the symmetric properties in $\phi_i-\phi'$ for each polarimetric quantity reveals that g'_h and g'_v should have only real valued $g'_{\gamma,n}$ which are even in n, while g'_U and g'_V should have only imaginary valued $g'_{\gamma,n}$ which are odd in n.

Using the Fourier expansion in (9) results in

$$\Delta T_\gamma = -T_s\left(\int_0^\infty d\beta\int_0^{2\pi} d\phi'\; C(k\beta,\phi')\cdot\sum_{n=-\infty}^{\infty} e^{in(\phi_i-\phi')}g'_{\gamma,n}(\beta)\right) \quad (13)$$

$$= -T_s\left(\sum_{n=-\infty}^{\infty} e^{in\phi_i}\int_0^\infty d\beta\; g'_{\gamma,n}(\beta)\cdot\int_0^{2\pi} d\phi'\; e^{-in\phi'}C(k\beta,\phi')\right) \quad (14)$$

$$= -T_s\left(\sum_{n=-\infty}^{\infty} e^{in\phi_i}\int_0^\infty d\beta\; g'_{\gamma,n}(\beta)C_n(k\beta)\right) \quad (15)$$

$$= -T_s\left(\begin{bmatrix}\int_0^\infty d\beta\; g'_{\gamma,0}(\beta)C_0(k\beta)\\ 0\end{bmatrix} + \sum_{n=1}^{\infty}\cdot\begin{bmatrix}2\cos(n\phi_i)\int_0^\infty d\beta\,\mathrm{Re}\{g'_{\gamma,n}(\beta)\}C_n(k\beta)\\ -2\sin(n\phi_i)\int_0^\infty d\beta\,\mathrm{Im}\{g'_{\gamma,n}(\beta)\}C_n(k\beta)\end{bmatrix}\right) \quad (16)$$

where the upper row in the final equality holds for h and v, the lower row for U and V, and an assumption that the curvature spectrum contains only cosine harmonics has been made. Equation (16) has separated out individual emission azimuthal harmonic terms (the $\cos(n\phi_i)$ and $\sin(n\phi_i)$ terms) and reveals them to be proportional to an integral of a weighting function $g'_{\gamma,n}(\beta)$ times the $C_n(k\beta)$ functions. Note that

$$C_n(k\beta) = \int_0^{2\pi} d\phi'\; e^{-in\phi'}C(k\beta,\phi') \quad (17)$$

represents the nth harmonic of the surface curvature spectrum, so the above equation demonstrates the direct correspondence between emission and surface azimuthal harmonics. Again, since the properties of a surface directional spectrum require it to have no odd azimuthal harmonics, the above equation clarifies that no odd emission harmonics will be obtained in this second order formulation. In addition, the above equation makes calculation of emission harmonics a much more direct procedure, since two single integrals [one for the Fourier series expansion of the g'_γ functions and the $d\beta$ integration in (16)] replace the multiple double integrals in an azimuth sweep procedure.

IV. Study of Weighting Functions

Plots of the harmonic weighting functions $g'_{\gamma,n}(\beta)$ for fixed values of θ_i and ϵ can help reveal the extent to which emission azimuth harmonics are sensitive to azimuthal anisotropy in varying ocean length scales. Note that plots of the weighting functions remove any influence of a particular ocean spectral model, since the total azimuthal harmonic is obtained by integrating the product of the weighting function with the corresponding surface harmonic coefficients. The large amount of uncertainty in the directional properties of the ocean spectrum, and in particular their variation with length scale, makes this a desirable procedure. Plots of the weighting functions will be made using logarithmic axes due to the large range of ocean length scales considered; however, use of logarithmic axes makes assessing contributions to the integrals in (16) difficult. Transforming the integration variable from β to $\log_{10}\beta$ eliminates this problem:

$$\int_0^\infty d\beta\;\mathrm{Re}\{g'_{\gamma,n}(\beta)\}C_n(k\beta) = (\ln 10)\int_{-\infty}^{\infty} d(\log_{10}\beta)\beta\;\mathrm{Re}\{g'_{\gamma,n}(\beta)\}C_n(k\beta). \quad (18)$$

Plots of $\beta\,\mathrm{Re}\{g'_{\gamma,n}(\beta)\}$ versus $\log_{10}\beta$ can thus be multiplied with plots of $C_n(k\beta)$ versus $\log_{10}\beta$ and integrated linearly over $\log_{10}\beta$ to obtain total harmonic contributions. Note also that use of a logarithmic axis for weighting function values will produce rapid nulls when the weighting functions cross through zero; however the wide range of possible weighting function values again makes a logarithmic axis useful.

Figs. 1–3 plot $\beta\,\mathrm{Re}\{g'_{\gamma,n}\}$ for h and v and $\beta\,\mathrm{Im}\{g'_{\gamma,n}\}$ for U and V versus $-\log_{10}\beta$ (the logarithm of ocean length scale relative to electromagnetic wavelength, expressed in terms of length on the plot axis) for observation angles of 0, 30, and 60°, respectively, and for $\epsilon = 39.7 + i40.2$ (approximate permittivity of sea water at 14 GHz [22]). Four plots are included in each figure: magnitudes of the zeroth and second harmonic weighting functions in dB and their signs, defined as $+1$ for positive values of $\mathrm{Re}\{g'_{\gamma,n}\}$ or $\mathrm{Im}\{g'_{\gamma,n}\}$ and -1 for negative values. Note the four sign functions are

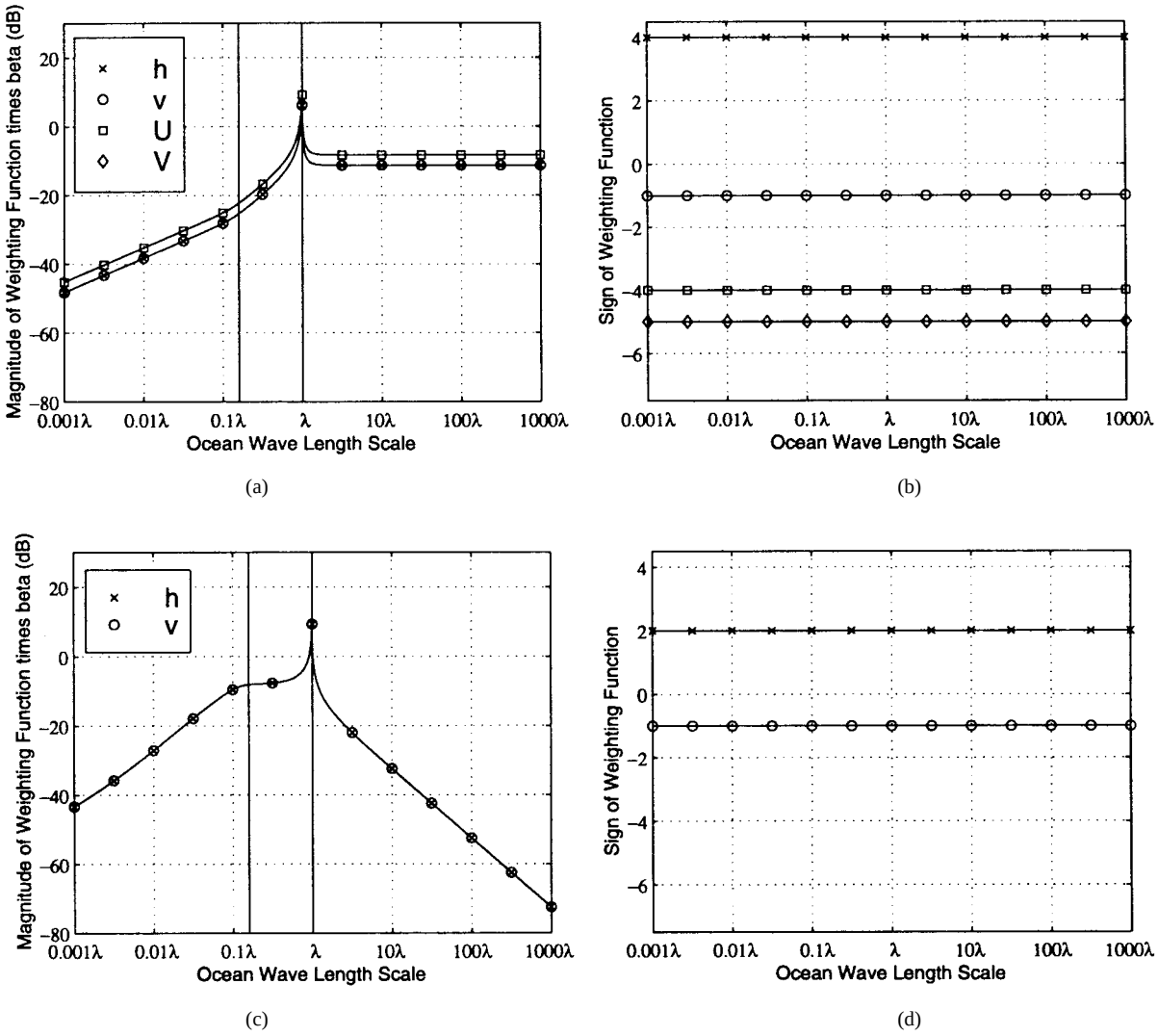

Fig. 1. Weighting functions for $\epsilon = 39.7 + i40.2$ and 0 degree observation angle (a) Magnitude of second harmonic weighting function. (b) Sign of second harmonic weighting function. (c) Magnitude of zeroth harmonic weighting function. (d) Sign of zeroth harmonic weighting function. Note that $\beta g_h^{'}$, $\beta g_U^{'}$, and $\beta g_V^{'}$ sign functions are shifted by $+3$, -3, and -6, respectively, to enable to curves to be distinguished.

shifted in steps of three to allow the curves to be more easily distinguished. In general in these curves, it is observed that the weighting functions are very smooth functions for length scales much greater than or much less than the electromagnetic wavelength, and clearly should reduce to simple expressions in terms of $1/\beta$. A general trend of constant valued curves for larger ocean length scales (small β) is observed as well, with the exception of $\beta g_{V,2}^{'}$ which falls off rapidly for large length scales. However, for length scales comparable to the electromagnetic wavelength, several resonance type behaviors are observed, particularly at larger observation angles. These resonance type behaviors can be attributed to a "critical phenomenon" effect [23], associated with scattered waves making a transition from propagating to nonpropagating, i.e., k_z crossing through 0 and becoming imaginary or k_{1z} reaching a minimum. Further study of this effect shows that only length scales in the ranges $\lambda/(1 \pm \sin\theta_i)$ and $\lambda/(\sqrt{\mathrm{Re}\{\epsilon\}} \pm \sin\theta_i)$ can show critical phenomena; the vertical lines in the figures indicate the outermost boundaries of these limits and confirm that the resonance effects are associated with critical phenomena. In this region, extreme care must be exercised in evaluating the weighting function harmonics from (12) due to rapid variations with azimuth; a total of 16 384 points in the azimuth integration were used to generate the figures shown. Note also that in or near the resonance region there can be sign changes in the weighting functions, showing that some length scales can work in opposition to each other in generating emission harmonics. Plots of the weighting functions for fourth and higher azimuthal harmonics can be generated as well, but since most models of ocean directional spectra do not predict higher than second azimuthal harmonics in the spectrum, no emission signatures would be obtained.

A few features of Fig. 1 are also worth noting. Since these plots are for observation at normal incidence, h and v weighting function magnitudes become identical, the U second harmonic weighting function magnitude is twice that of h or v, and the V second harmonic weighting function becomes zero. Second harmonic weighting functions in Fig. 1 are particularly simple, with only one critical phenomenon occurring at the electromagnetic wavelength. Zeroth harmonic

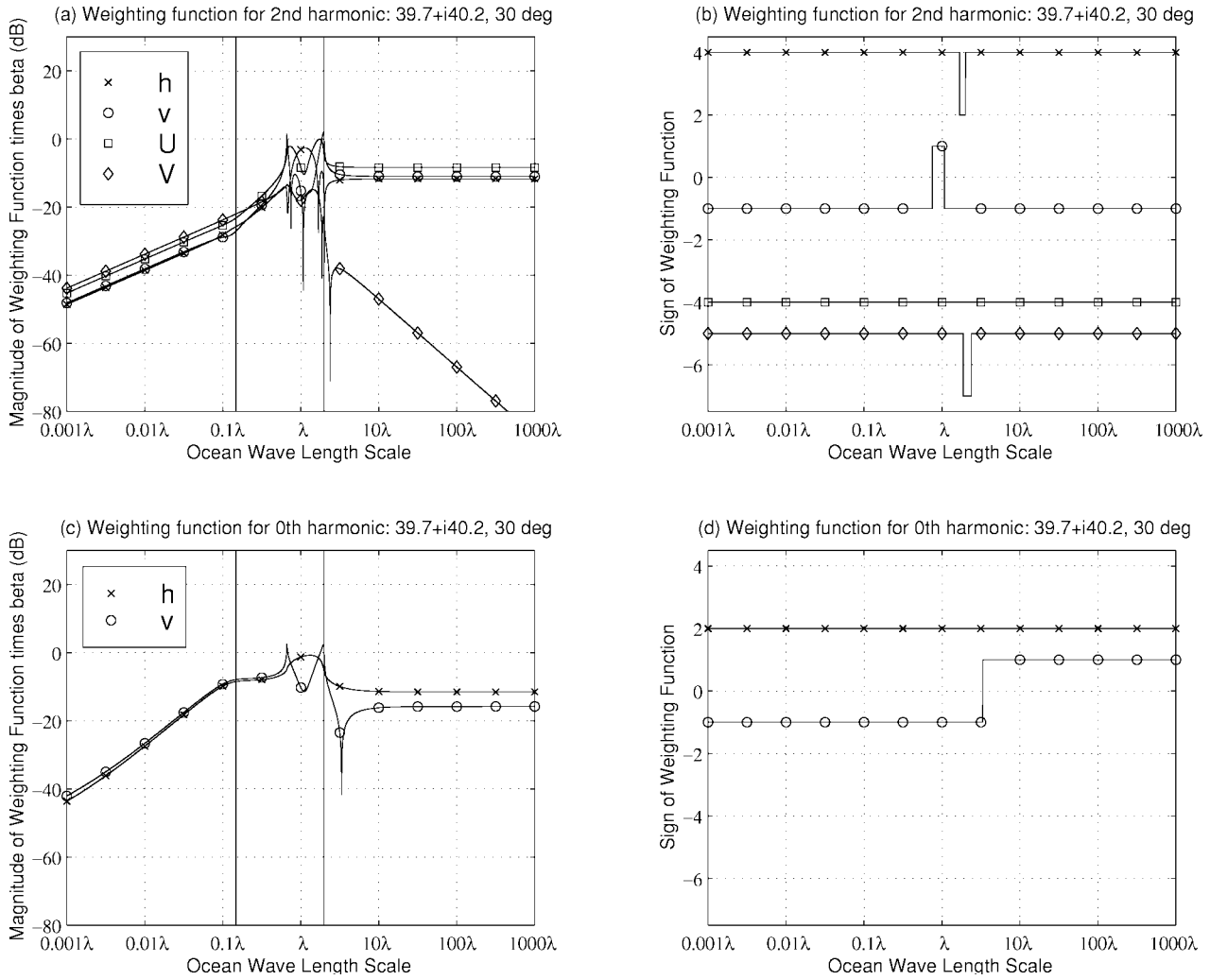

Fig. 2. Same as Fig. 1 but for 30° observation angle.

weighting functions (never plotted for U and V since these quantities identically have no zeroth harmonic) are also interesting, since they indicate that the zeroth harmonic at normal incidence is dominated only by ocean length scales equal to the electromagnetic wavelength. Zeroth harmonics at oblique observation however show contributions from length scales both larger and smaller than λ.

Similar plots can be made for other observation angles and values of surface relative permittivity, and show similar behaviors. Some differences occur in the case when the surface relative permittivity is purely real, but since this is not realistic for the ocean at microwave frequencies, this case will not be further discussed. Overall, plots of these weighting functions show that emission second harmonics predicted by the SPM/SSA are sensitive (with the exception of V) to anisotropy in ocean length scales much larger than λ, as indicated by the constant valued weighting functions. However, the resonance behaviors observed in the critical phenomena region produce a significant sensitivity to ocean length scales on the order of λ as well. Of course, obtaining a final prediction of emission second harmonics requires inclusion of an ocean directional spectrum model, and the product of the weighting function and ocean curvature spectrum harmonics may result in either large or mid range length scales being the dominant contributor to emission harmonics. Fig. 4 plots zeroth and second harmonic coefficients of curvature spectra obtained from two ocean spectral models at wind speed 10 m/s: that of Durden–Vesecky [21] and a symmetrized Apel spectrum [24]. Note that these two models place surface azimuthal anisotropy in differing length scales, with the Apel spectrum emphasizing more the azimuthal anisotropy of longer gravity waves. Prediction of emission second harmonics simply requires shifting the curvature spectrum harmonic functions so that the appropriate length scale is aligned with λ in the weighting function plot, and then integrating the product of the two curves over $\log_{10}\beta$. This procedure clearly shows that the Apel spectrum would result in much larger azimuthal harmonic predictions at low frequencies than would the Durden–Vesecky model. The exact directional dependence of the ocean surface spectrum remains a subject of research.

V. Approximation for Large Scale Wave Contributions

An examination of the curves of Figs. 1–3 reveals them to remain constant for length scales much greater than λ. A $1/\beta$ dependence of the $g'_{\gamma,n}$ functions for β small can also

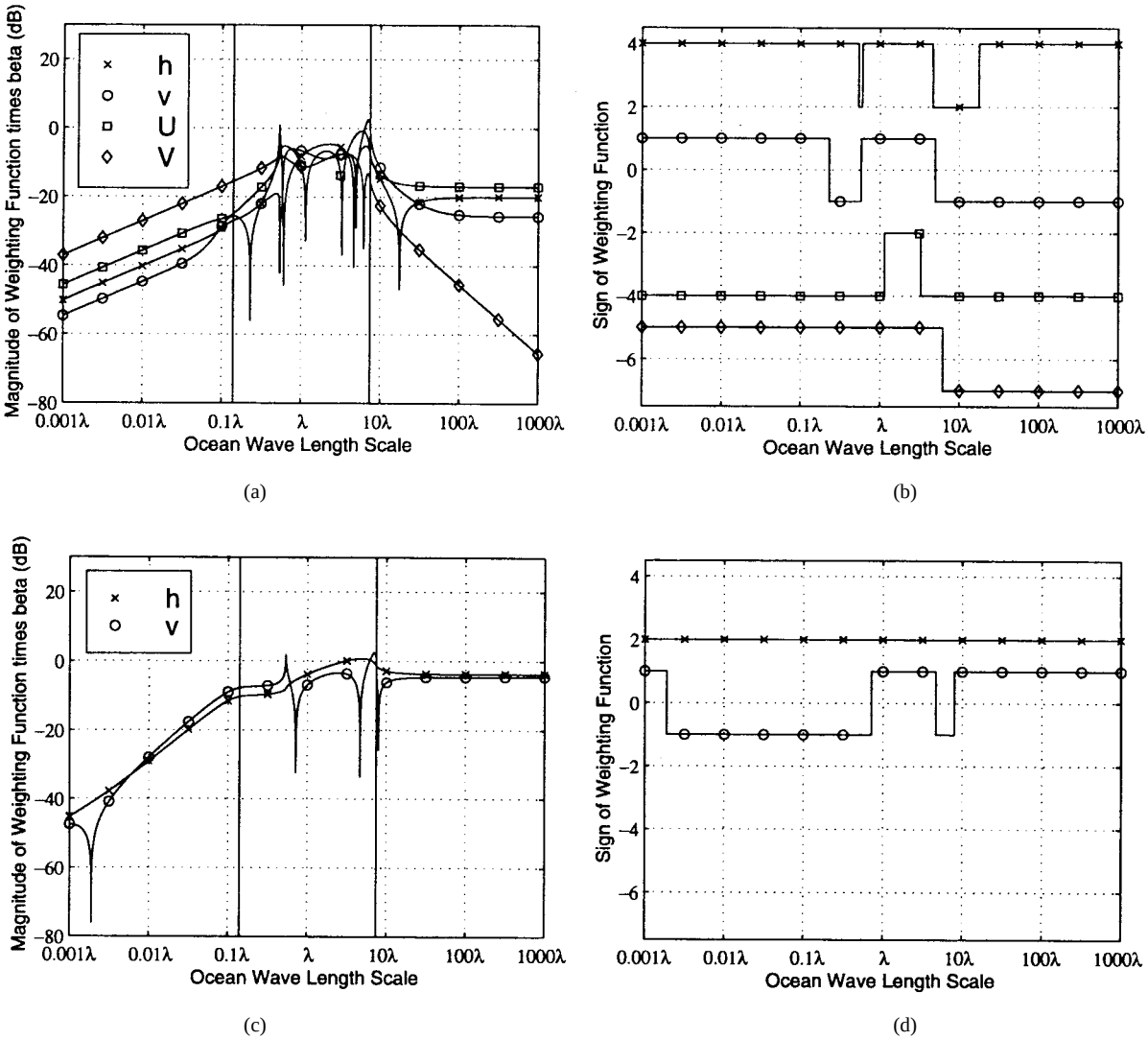

Fig. 3. Same as Fig. 1 but for 60° observation angle.

be derived in general through an expansion of the weighting function in β. It is more convenient to illustrate this expansion in terms of the original g_γ functions of (4)–(7). Small values of β indicate small values of $k_\rho^{'}$ or large length scale waves in the ocean spectrum. Since the values of k_x, k_y, and k_z used in the first and second order scattering coefficients are found through $k_x = k_{xi} + k_\rho^{'}\cos\phi^{'}$, $k_y = k_{yi} + k_\rho^{'}\sin\phi^{'}$, and $k_z = \sqrt{k^2 - k_x^2 - k_y^2}$, an expansion assuming $k_\rho^{'}$ is small produces

$$k_z \approx k_{zi} - \frac{k_{\rho i}k_\rho^{'}}{k_{zi}}\cos(\phi_i - \phi^{'}) - \frac{k_\rho^{'2}}{2k_{zi}} \cdot \left(1 + \frac{k_{\rho i}^2}{k_{zi}^2}\cos^2(\phi_i - \phi^{'})\right) \tag{19}$$

to second order in $k_\rho^{'}$. Similar expansions can be made for all terms in the first and second order scattering coefficients, and terms multiplying powers of $k_\rho^{'}$ can be collected in the g_γ functions. It is found that zeroth and first order terms both produce no emission contributions for a surface spectrum containing only even cosine harmonics; terms in $k_\rho^{'2}$ yield the first nonzero result. Overall it can be shown that the form of the g_γ functions in this limit is

$$g_\gamma \approx k_\rho^{'2}\left(\begin{bmatrix} h_{\gamma,l}^{(0)}(\theta_i,\epsilon) \\ 0 \end{bmatrix} + \begin{bmatrix} h_{\gamma,l}^{(2)}(\theta_i,\epsilon)\cos(2\phi_i)\cos(2\phi^{'}) \\ h_{\gamma,l}^{(2)}(\theta_i,\epsilon)\sin(2\phi_i)\cos(2\phi^{'}) \end{bmatrix}\right) \tag{20}$$

where $h_{\gamma,l}^{(0)}(\theta_i,\epsilon)$ and $h_{\gamma,l}^{(2)}(\theta_i,\epsilon)$ are now constants in $k_\rho^{'}$ and $\phi^{'}$; the subscript l denotes "long" waves and the superscript indicates the azimuthal dependency generated by the function. The upper row in the above equation is used with h and v brightnesses; the lower row with U and V. Since these expressions hold for the original g_γ functions, which did depend on frequency in general, it is clear from the above expression that the only frequency dependence of long wave contributions to either zeroth or second emission azimuthal harmonics is permittivity related.

The dependencies obtained in the long wave limit are particularly appealing because when used in (3) they produce

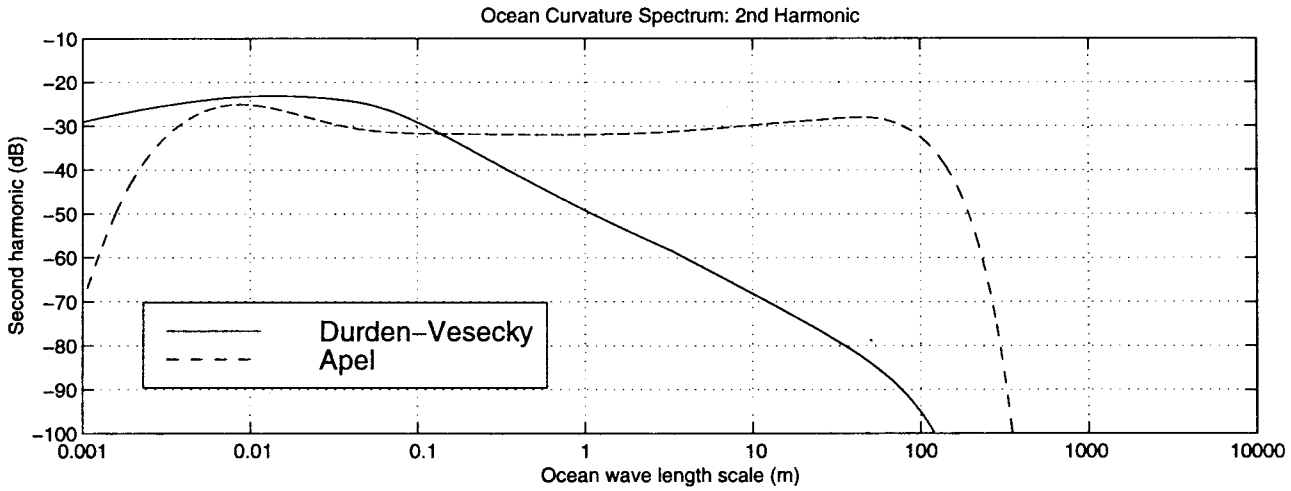

(a)

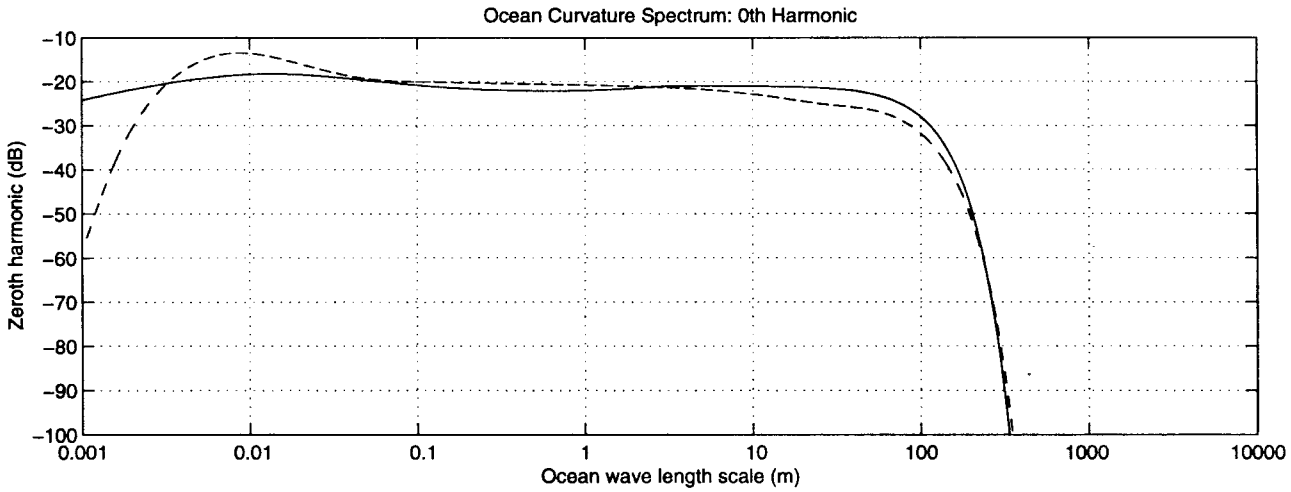

(b)

Fig. 4. Zeroth and second harmonic coefficients of curvature spectrum $C_n(k_\rho')$ for Durden–Vesecky and Apel models. (a) Second harmonics. (b) Zeroth harmonics.

$$\Delta T_\gamma = -T_s\left(\int_0^{k_m} dk_\rho'\, k_\rho' \int_0^{2\pi} d\phi'\, W(k_\rho',\phi') \cdot g_\gamma(f,\theta_i,\phi_i,\epsilon,k_\rho',\phi')\right) \tag{21}$$

$$= -T_s\left(\int_0^{k_m} dk_\rho'\, k_\rho' \int_0^{2\pi} d\phi'\, W(k_\rho',\phi')k_\rho'^2 \cdot \left\{\begin{bmatrix} h_{\gamma,l}^{(0)}(\theta_i,\epsilon) \\ 0 \end{bmatrix} + \begin{bmatrix} h_{\gamma,l}^{(2)}(\theta_i,\epsilon)\cos(2\phi_i)\cos(2\phi') \\ h_{\gamma,l}^{(2)}(\theta_i,\epsilon)\sin(2\phi_i)\cos(2\phi') \end{bmatrix}\right\}\right)$$

$$= -T_s\left(\begin{bmatrix} S^2 h_{\gamma,l}^{(0)}(\theta_i,\epsilon) \\ 0 \end{bmatrix} + (S_x^2 - S_y^2) \cdot \begin{bmatrix} h_{\gamma,l}^{(2)}(\theta_i,\epsilon)\cos(2\phi_i) \\ h_{\gamma,l}^{(2)}(\theta_i,\epsilon)\sin(2\phi_i) \end{bmatrix}\right) \tag{22}$$

where S_x^2 and S_y^2 are the long wave surface slope variances in the x and y directions respectively and $S^2 = S_x^2 + S_y^2$ is the total surface slope variance. This result shows that long wave emission zeroth and second azimuthal harmonic contributions are directly proportional to the long wave slope anisotropy, and that the dependence of the long wave contributions on polar observation angle θ_i is completely determined by the surface relative permittivity through the $h_{\gamma,l}$ functions. Note that the k_ρ' integration in the above equations is truncated at k_m to include only the long wave region; this region should be chosen to be well outside the critical phenomenon limit described previously.

Although the $h_{\gamma,l}^{(0)}(\theta_i,\epsilon)$ and $h_{\gamma,l}^{(2)}(\theta_i,\epsilon)$ functions can be derived analytically through the k_ρ' expansion, the resulting functions are quite complicated and so are not presented here. It is found that $h_{V,l}^{(2)}(\theta_i,\epsilon) = 0$ as expected from Figs. 1–3. Rewriting (22) as

$$\Delta T_\gamma = -T_s\left(\begin{bmatrix} S^2 h_{\gamma,l}^{(0)}(\theta_i,\epsilon) \\ 0 \end{bmatrix} + S^2\frac{S_x^2 - S_y^2}{S_x^2 + S_y^2} \cdot \begin{bmatrix} h_{\gamma,l}^{(2)}(\theta_i,\epsilon)\cos(2\phi_i) \\ h_{\gamma,l}^{(2)}(\theta_i,\epsilon)\sin(2\phi_i) \end{bmatrix}\right) \tag{23}$$

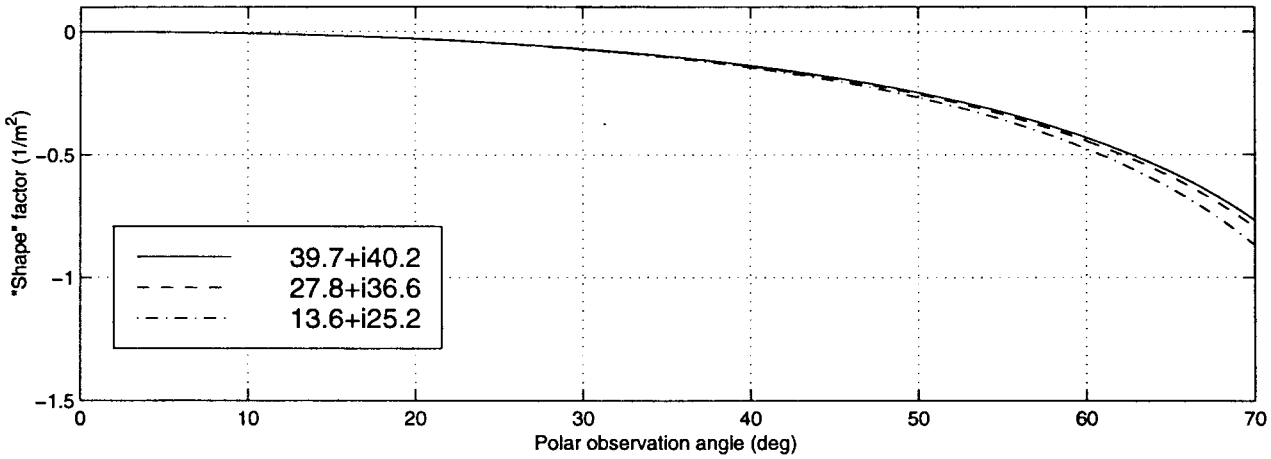

(a)

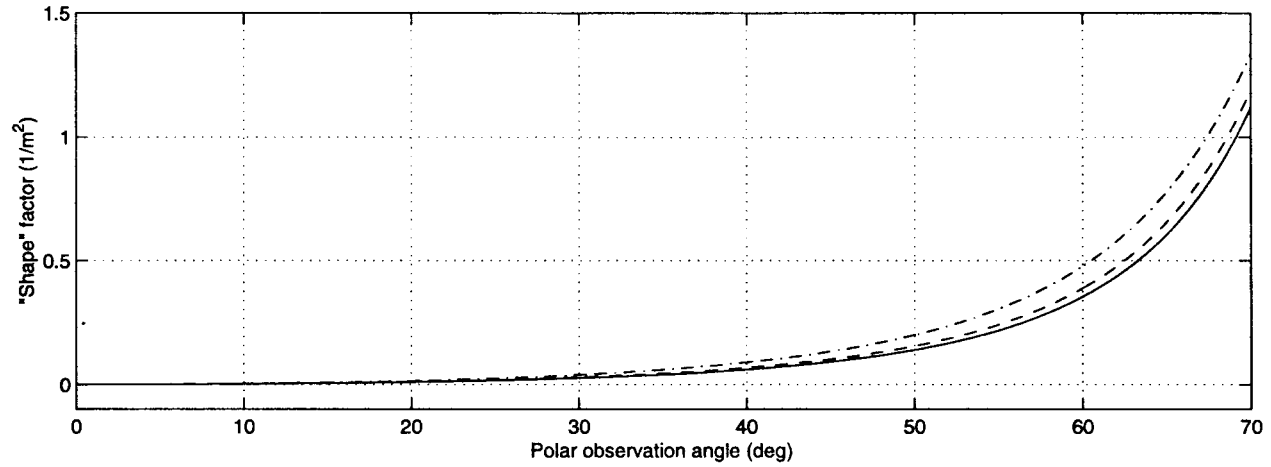

(b)

Fig. 5. Long wave zeroth harmonic "shape" factors $h^{(0)}_{\gamma,l}(\theta_i,\epsilon)$ versus polar observation angle θ_i for sea water permittivities at 14, 19, and 35 GHz. (a) Horizontal. (b) Vertical.

shows that long wave second harmonic contributions can be expressed as a product of three factors: the long wave total slope variance, S^2, a slope asymmetry factor, $(S_x^2-S_y^2)/(S_x^2+S_y^2)$, and the "shape" versus polar observation angle functions, $h^{(2)}_{\gamma,l}(\theta_i,\epsilon)$, again which are independent of frequency and the surface geometry.

The observed dependence on surface slope only confirms the small slope approximation, and it is clear that increases in total long wave slope variance for a fixed upwind to cross wind slope variance ratio results in increasing second harmonics. The asymmetry factor correctly reduces to zero for an isotropic spectrum, and is seen to vary between minus one and one with a fairly rapid saturation as the up wind to cross wind slope ratio increases. Figs. 5 and 6 plot the zeroth harmonic and second harmonic"shape" factors respectively for three surface permittivities, corresponding to approximate permittivities of sea water at 14, 19, and 35 GHz [22]. The characteristic variations of emission second harmonics observed in measurements are seen in these figures, with a zero crossing occurring in the 50–60 degree polar observation angle range, which varies with surface permittivity. Note V terms are also included from the exact weighting functions, but they are extremely small and can be neglected. It is seen that long wave zeroth harmonic contributions are zero near normal incidence, as in Fig. 1, and increase in magnitude at oblique incidence.

Depending on the ocean spectrum model chosen and the operating frequency, the long wave portion may or may not contribute significantly to ocean azimuthal harmonics. The above equation reveals the simple dependence of these contributions on long wave slope variances. A dependence on surface slope alone is similar to what might be expected from a geometrical optics emission calculation, and numerical studies [16] have confirmed that both PO [11] and SPM based emission calculations yield accurate results for large scale surface features. It is interesting to observe that an SPM based emission formulation reduces to the physical optics limit for large height but small sloped surfaces! The relatively simple integral expressions of the SPM/SSA method however make obtaining the above approximations for long wave contributions much simpler and clarify the limitations of the approximation. In addition, the approximate expression

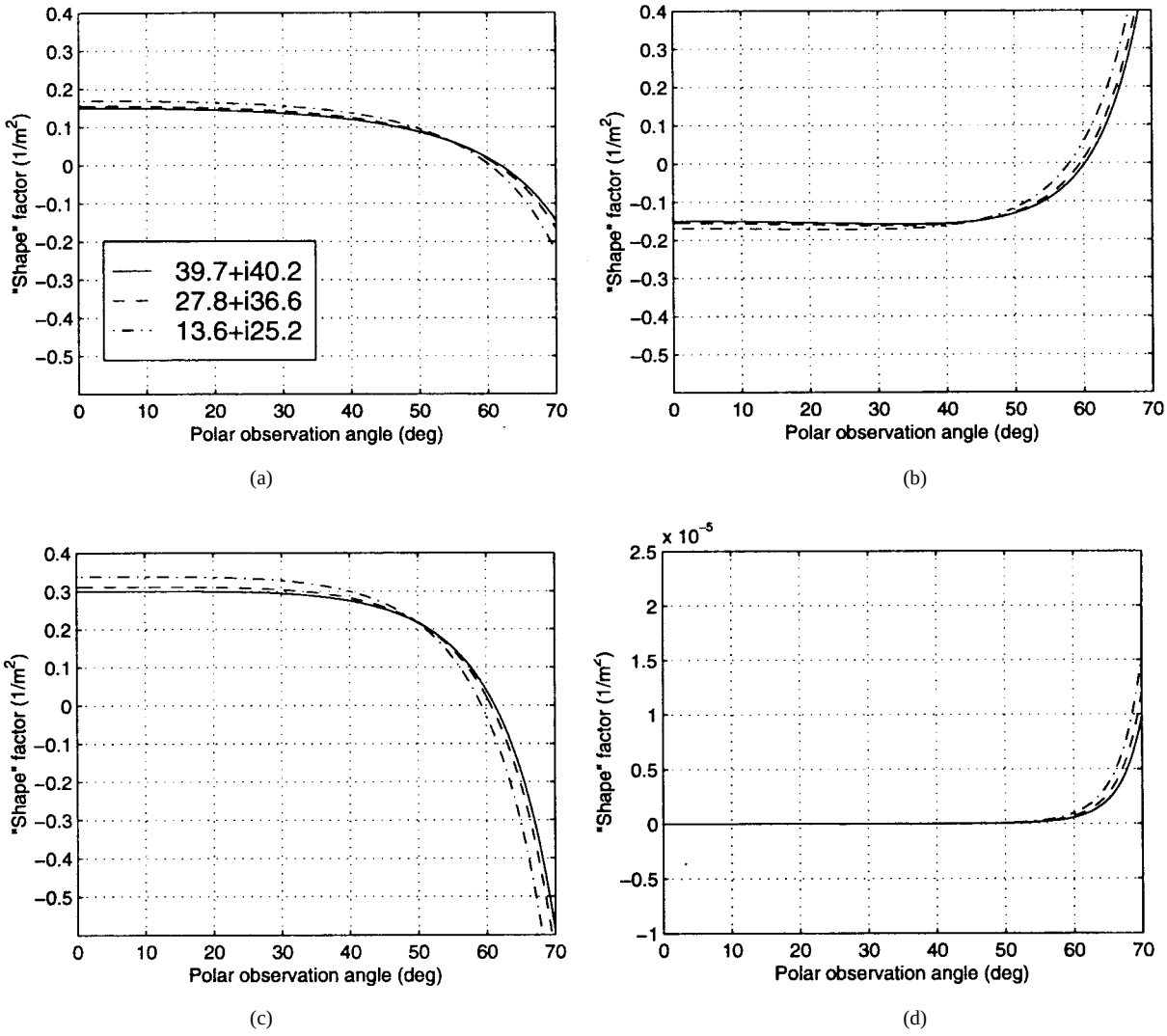

Fig. 6. Long wave second harmonic "shape" factors $h^{(2)}_{\gamma,l}(\theta_i,\epsilon)$ versus polar observation angle θ_i for sea water permittivities at 14, 19, and 35 GHz. (a) Horizontal. (b) Vertical. (c) U. (d) V.

presented can be used to increase the efficiency of emission harmonic calculations for the full spectrum, since only a calculation of long wave slope variances is required to obtain all long wave contributions.

VI. Approximation for Small Scale Wave Contributions

A similar expansion can be made for length scales much smaller than $\lambda/(\sqrt{\mathrm{Re}\{\epsilon\}}+\sin\theta_i)$, again as seen in Figs. 1–3 where the weighting functions become smooth for small length scales. In this case the expansion assumes large values of k_ρ', so that an expansion in $k_{\rho i}/k_z'$ is obtained:

$$k_z \approx k_z' - \frac{k_\rho' k_{\rho i}}{k_z'}\cos(\phi_i-\phi') - \frac{k_{\rho i}^2}{2k_z'} \cdot \left(1+\frac{k_\rho'^2}{k_z'^2}\cos^2(\phi_i-\phi')\right) \tag{24}$$

where $k_z' = \sqrt{k^2-k_\rho'^2}$. In this case it is found that zeroth order in $k_{\rho i}$ terms contribute to emission azimuthal harmonics if the surface permittivity has an imaginary part. It can be shown for very short waves (again significantly outside the critical phenomena region for the sea water region) that the g_γ second harmonic weighting functions approach a function which varies as $k_\rho'^2(k/k_\rho')$, so that a direct dependence on short wave surface slope variances is not obtained. Instead the result can be written as

$$\begin{aligned}\Delta T_\gamma^{(2)} &= -T_s\left(\int_{k_n}^{\infty} dk_\rho'\, k_\rho' \int_0^{2\pi} d\phi'\, W(k_\rho',\phi')k_\rho'^2\left(\frac{k}{k_\rho'}\right)\right. \\ &\quad \left.\cdot \begin{bmatrix} h^{(2)}_{\gamma,s}(\theta_i,\epsilon)\cos(2\phi_i)\cos(2\phi') \\ h^{(2)}_{\gamma,s}(\theta_i,\epsilon)\sin(2\phi_i)\cos(2\phi')\end{bmatrix}\right) \\ &= -T_s\left((S_x'^2 - S_y'^2)\begin{bmatrix} h^{(2)}_{\gamma,s}(\theta_i,\epsilon)\cos(2\phi_i) \\ h^{(2)}_{\gamma,s}(\theta_i,\epsilon)\sin(2\phi_i)\end{bmatrix}\right)\end{aligned} \tag{25}$$

where the s subscript on the $h_{\gamma,s}$ functions now stands for "short" waves, and the $S_x'^2$, $S_y'^2$, and $S'^2 = S_x'^2 + S_y'^2$ are "modified" short wave slope variances in that they are calculated with a filtering function k/k_ρ' included. Since k_ρ' is assumed to be large in this limit, the filtering function shows a de-emphasis on the contributions of short scale waves

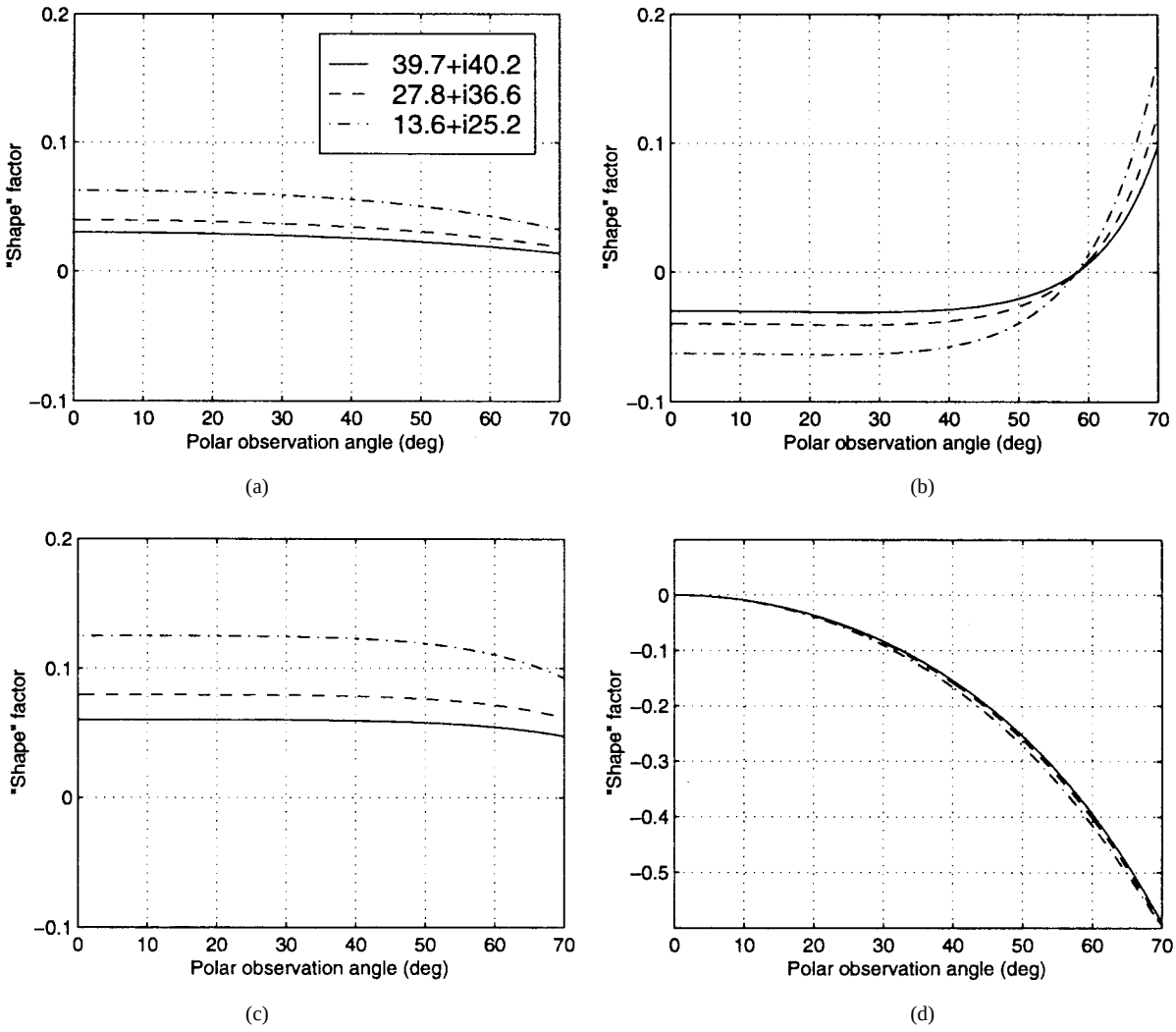

Fig. 7. Short wave second harmonic "shape" factors $h^{(2)}_{\gamma,s}(\theta_i,\epsilon)$ versus polar observation angle θ_i for sea water permittivities at 14, 19, and 35 GHz. (a) Horizontal. (b) Vertical. (c) U. (d) V.

in the SPM/SSA emission process. Zeroth harmonic terms in the short wave limit are more complex, involving terms proportional to the short wave surface variance and modified surface slope, and so are not presented here. Note even though a surface variance dependence is obtained, these contributions occur only for length scales much shorter than λ for which small slopes also imply very small heights relative to λ; the overall expansion can thus still be considered a small slope approximation.

Fig. 7 plots second harmonic "shape" factors analogously to Fig. 6. Note overall that the short wave contributions have smaller values of the slope-dependent "shape" factor than the long waves, with the exception of $h^{(2)}_{V,s}$, which has no long wave contributions. Clearly the weighting functions demonstrate that the V_B brightness has the most sensitivity to short scale waves on the ocean surface. Again these approximations can be useful in calculating emission harmonics more efficiently.

VII. Discussion

The results of this paper clarify the physics of the emission process predicted by the SPM/SSA, independent of a particular directional spectrum model for the ocean surface. Use of an azimuthal Fourier series enabled the sources of individual emission harmonics to be identified as an integral of the corresponding surface spectrum harmonic with a distinct weighting function for each harmonic and polarimetric brightness. These weighting functions were found to be sensitive to length scales much larger than the electromagnetic wavelength, with the exception of the V_B term, although significant sensitivities to length scales within an order of magnitude of the electromagnetic wavelength were also observed. The fourth Stokes brightness, V_B was found to be the most sensitive of the four brightnesses to small scale features in the ocean spectrum, and an interesting sensitivity of nadir viewing zeroth harmonic T_{Bh} brightness to a single scale in the ocean spectrum was observed. Consideration of these results clarifies the fact that previous works have concluded that the short gravity/capillary wave portion of the spectrum dominated emission second harmonics due to use of the Durden–Vesecky ocean spectrum, which places most of the azimuthal anisotropy in these length scales. However, the weighting functions show that large scale waves can also contribute if they are anisotropic.

Approximations to the weighting functions in the large wave and short wave limits produced simple equations for emission zeroth and second azimuthal harmonics in terms of a product of the surface standard or modified slope variance with an asymmetry factor and a "shape" factor which was independent of surface geometry and completely determined the dependence of the harmonic coefficients on polar observation angle. These approximations again show that long wave contributions can be significant, and can also be used to improve the efficiency of brightness temperature calculations. A physical or geometrical optics approximation should also be appropriate for these contributions, but would become inaccurate for wavelength and sub-wavelength scale effects.

The success of the SPM/SSA in matching measured brightness temperature harmonics [10] has shown that the technique should be applicable for ocean brightness temperature predictions. Remaining issues involve a more complete study of the third order expansion, so that emission first azimuthal harmonics can be obtained, as well as the effects of foam and atmospheric emissions. In addition, the dependence of ocean surface anisotropy on length scale remains an open question, as evidenced by the differing predictions of the two spectral models considered in this paper. Finally, consideration of the weighting functions presented in this paper can enable combinations of polarimetric brightness quantities to be designed to obtain enhanced sensitivities to particular ocean length scales for remote sensing applications; the sensitivity of nadir viewing zeroth harmonic brightness temperatures to a single ocean surface length scale clearly suggests such possibilities.

REFERENCES

[1] M. S. Dzura, V. S. Etkin, A. S. Khrupin, M. N. Pospelov, and M. D. Raev, "Radiometers polarimeters: Principles of design and applications for sea surface microwave emission polarimetry," in *Proc. IGARSS'92*, pp. 1432–1434.

[2] F. J. Wentz, "Measurement of oceanic wind vector using satellite microwave radiometers," *IEEE Trans. Geosci. Remote Sensing*, vol. 30, pp. 960–972, 1992.

[3] S. H. Yueh, W. J. Wilson, F. K. Li, S. V. Nghiem, and W. B. Ricketts, "Polarimetric measurements of sea surface brightness temperatures using an aircraft K-band radiometer," *IEEE Trans. Geosci. Remote Sensing*, vol. 33, pp. 85–92, 1995.

[4] S. H. Yueh, W. J. Wilson, and R. West, "Ocean surface wind remote sensing using microwave backscatter and brightness temperatures," in *Proc. IGARSS'98*, vol. 5, pp. 2321–2323.

[5] K. St. Germain, G. Poe, P. and Gaiser, "Modeling of the polarimetric microwave signal due to ocean surface wind vector," in *Proc. IGARSS'98*, vol. 5, pp. 2304–2306.

[6] J. R. Piepmeier, A. J. Gasiewski, M. Klein, V. Boehm, and R. C. Lum, "Ocean surface wind direction measurement by scanning polarimetric microwave radiometry," in *Proc. IGARSS'98*, vol. 5, pp. 2307–2310.

[7] V. G. Irisov and Y. G. Trokhimovski, "Observation of the ocean brightness temperature anisotropy during the coastal ocean probing experiment," in *Proc. IGARSS'96*, vol. 3, pp. 1457–1459.

[8] S. D. Gasster and G. M. Flaming, "Overview of the conical microwave imager/sounder development for the NPOESS program," in *Proc. IGARSS'98*, vol. 1, pp. 268–271, 1998.

[9] S. H. Yueh, R. Kwok, F. K. Li, S. V. Nghiem, and W. J. Wilson, "Polarimetric passive remote sensing of ocean wind vectors," *Radio Sci.*, vol. 29, pp. 799–814, 1994.

[10] S. H. Yueh, "Modeling of wind direction signals in polarimetric sea surface brightness temperatures," *IEEE Trans. Geosci. Remote Sensing*, vol. 35, pp. 1400–1418, 1997.

[11] D. B. Kunkee and A. J. Gasiewski, "Simulation of passive microwave wind direction signatures over the ocean using an asymmetric-wave geometrical optics model," *Radio Sci.*, vol. 32, p. 59, 1997.

[12] V. G. Irisov, "Small-slope expansion for thermal and reflected radiation from a rough surface," *Waves Random Media*, vol. 7, pp. 1–10, 1997.

[13] ——, "Microwave radiation from a weakly nongaussian surface," in *Proc. IGARSS'98* vol. 5, pp. 2329–2332.

[14] J. T. Johnson, R. T. Shin, L. Tsang, K. Pak, and J. A. Kong, "A numerical study of ocean polarimetric thermal emission," *IEEE Trans. Geosci. Remote Sensing*, vol. 37, pp. 8–20, Jan. 1999.

[15] A. G. Voronovich, *Wave Scattering from Rough Surfaces*. Berlin, Germany: Springer-Verlag, 1994.

[16] M. Zhang and J. T. Johnson, "Theoretical studies of ocean polarimetric brightness signatures," in *Proc. IGARSS'98*, vol. 5, pp. 2333–2335.

[17] M. L. Van Woert, "The AEOLIS program: Prospects for future, low-cost, space-borne vector wind sensors," in *Proc. IGARSS'96*, pp. 1117–1119.

[18] L. Tsang, J. A. Kong, and R. T. Shin, *Theory of Microwave Remote Sensing*. New York: Wiley, 1985

[19] S. H. Yueh, R. Kwok, and S. V. Nghiem, "Polarimetric scattering and emission properties of targets with reflection symmetry," *Radio Sci.*, vol. 29, pp. 1409–1420, 1994.

[20] F. T. Ulaby, R. K. Moore, and A. K. Fung, *Microwave Remote Sensing*, vol. 2. Reading, MA: Addison-Wesley, 1982.

[21] S. L. Durden and J. F. Vesecky, "A physical radar cross-section model for a wind driven sea with swell," *IEEE J. Oceanic Eng.*, vol. OE-10, pp. 445–451, 1985.

[22] L. A. Klein and C. T. Swift, "An improved model for the dielectric constant of sea water at microwave frequencies," *IEEE Trans. Antennas Propagat.*, vol. AP-25, pp. 104–111, 1977.

[23] V. S. Etkin, N. N. Vorsin, Yu. A. Kravtsov, V. G. Mirovskii, V. V. Nikitin, A. E. Popov, and I. A. Troitskii, "Critical phenomena with the thermal radio irradiation of a periodically uneven water surface," *Izvestiya: Radiophys. Quant. Electron.*, vol. 21, pp. 316–318, 1978.

[24] J. R. Apel, "An improved model of the ocean surface wave vector spectrum and its effects on radar backscatter," *J. Geophys. Res.*, vol. 99, pp. 16269–16291, 1994.

Joel T. Johnson (M'96) received the B.E.E. degree from the Georgia Institute of Technology, Atlanta, in 1991 and the S.M. and Ph.D. degrees from the Massachusetts Institute of Technology, Cambridge, in 1993 and 1996, respectively.

He is currently an Assistant Professor, Department of Electrical Engineering and ElectroScience Laboratory, The Ohio State University, Columbus. His research interests are in the areas of microwave remote sensing, propagation, and electromagnetic wave theory.

Dr. Johnson is an associate member of commissions B and F of the International Union of Radio Science (URSI), and a member of Tau Beta Pi, Eta Kappa Nu, and Phi Kappa Phi. He received the 1993 best paper award from the IEEE Geoscience and Remote Sensing Society, and was named an Office of Naval Research Young Investigator, National Science Foundation Career awardee, and PECASE award recipient in 1997.

Min Zhang was born in Wuhan, China. She received the B.S.E.E. degree in 1996 from Huazhong University of Science and Technology, Wuhan, and the M.S.E.E. degree in 1999 from The Ohio State University (OSU), Columbus.

Since 1997, she has been a Graduate Rresearch Associate, ElectroScience Laboratory, OSU. Her research interests are in the area of microwave remote sensing, both active and passive.